C. R. Mecanique 347 (2019) 953–966

Contents lists available at ScienceDirect

Comptes Rendus Mecanique

www.sciencedirect.com

Nonlinear vibration analysis of piezoelectric bending actuators: Theoretical and experimental studies

Pouyan Shahabi, Hamed Ghafarirad, Afshin Taghvaeipour *

Mechanical Engineering Department, Amirkabir University of Technology (Tehran Polytechnic), Tehran, Iran

ARTICLE INFO

Article history:
Received 30 April 2019
Accepted 31 October 2019
Available online 26 November 2019

Keywords:
Piezoelectric bending actuator
Euler–Bernoulli beam theory
Nonlinear behavior
Multiple scales

ABSTRACT

Piezoelectric bimorph actuators are used in a variety of applications, including micro positioning, vibration control, and micro robotics. The nature of the aforementioned applications calls for the dynamic characteristics identification of actuator at the embodiment design stage. For decades, many linear models have been presented to describe the dynamic behavior of this type of actuators; however, in many situations, such as resonant actuation, the piezoelectric actuators exhibit a softening nonlinear behavior; hence, an accurate dynamic model is demanded to properly predict the nonlinearity. In this study, first, the nonlinear stress–strain relationship of a piezoelectric material at high frequencies is modified. Then, based on the obtained constitutive equations and Euler–Bernoulli beam theory, a continuous nonlinear dynamic model for a piezoelectric bending actuator is presented. Next, the method of multiple scales is used to solve the discretized nonlinear differential equations. Finally, the results are compared with the ones obtained experimentally and nonlinear parameters are identified considering frequency response and phase response simultaneously. Also, in order to evaluate the accuracy of the proposed model, it is tested out of the identification range as well.

1. Introduction

Demand for smart structures, such as piezoelectric ceramics, has attracted the attention of researchers for many years. These smart materials are mostly used as various type of position, force and mass sensors [1–3] and also energy harvesters [4,5]. In addition, piezoelectric actuators (PEAs) have been used in micro-manipulation [6,7], medical equipment [8,9] and position control applications [10,11].

Many researches targeted the linear dynamic modeling of piezoelectric actuators and sensors [12–15]. They believe that linear constitutive equations are sufficiently accurate for actuators that are experiencing weak electrical fields or small-amplitude strains. Accordingly, linear dynamic models are suggested for energy harvesting by piezoelectric cantilevers [13, 14]. In this regard, Hosseini and Hamedi presented an analytical model for linear piezoelectric energy harvesters; the governing equations were solved by resorting to the distributed parameter method. The authors then validated the model with the experimental data as well [16]. Raju and Umpathy also proposed a linear model for tapered piezoelectric beam with cavity. They obtained the natural frequencies and corresponding mode shapes of a piezoelectric energy harvester based on the Euler–Bernoulli beam theory, which were finally solved by Bessel functions [17].

* Corresponding author.
E-mail address: ataghvaei@aut.ac.ir (A. Taghvaeipour).

https://doi.org/10.1016/j.crme.2019.10.007
1631-0721/

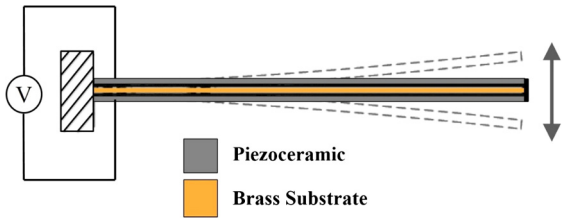

Fig. 1. Illustration of a series type bimorph actuator connected to a power supply.

Indeed, piezoelectric actuators show nonlinear behavior by increasing the electric field or working frequency. By increasing the input voltage, hysteresis nonlinear behavior will appear between input voltage and actuator position. Several conventional methods, such as Preisach, Prandtl Ishlinskii, Bouc Wen, etc., have been proposed to modify the dynamic model at high voltages [15,18,19].

However, piezoelectric actuators may exhibit nonlinear behaviors around the natural frequencies even for low amplitude input voltages. At these frequencies, conventional linear constitutive equations cannot express the actuator behavior accurately. In fact, material nonlinearities should be taken into account by proposing appropriate nonlinear constitutive equations. Because the nonlinear constitutive equations depend significantly on dimensions, electrical input amplitude, strain magnitude, etc., for a certain actuator, these equations should be obtained empirically.

Stanton et al. investigated the nonlinear energy harvesting of piezoelectric cantilevered beam comprehensively [20]. Based on energy methods, they suggested a dynamic model whose unknown nonlinear parameters were determined when the base of the piezoelectric beam is excited near its resonance. At the end, the authors reported that the linear damping model cannot describe the behavior of a piezoelectric cantilevered beam at high frequencies. As an alternative, a quadratic fluid damping was proposed to model the energy dissipation at high frequencies. Stanton et al. also tried to predict the nonlinear non-conservative behavior of piezoelectric energy harvesters with a proof mass at the tip of beam [21]. The authors proposed a deflection-dependent damping model for the system [21]. Recently, Erturk and Leadenham studied a nonlinear model for piezoelectric bimorph cantilevered beam. The authors investigated the piezo beam behavior under electrical and mechanical excitations for different applications such as energy harvesting, sensing and actuating [22]. In addition, Erturk and Tan investigated the nonlinear elastodynamics of piezoelectric macro-fiber composites with integrated electrodes for resonant actuation. In order to eliminate nonlinear fluid damping effects, they used an in vacuo actuation scenario under a broad range of voltage levels. A mathematical model is obtained using the harmonic balance method [23].

A majority of the past studies are concerned about piezoelectric energy harvesters that are excited by the base vibration but, in the present work, the nonlinear behavior of a piezoelectric bimorph actuator is investigated; hence, it is excited by means of the applied voltage. In this regard, first, the nonlinear stress–strain relationship for piezoelectric materials at high frequencies, which was previously presented in [24], is effectively modified. Then, based on the obtained constitutive equations and Euler–Bernoulli beam theory, a nonlinear dynamic model for a piezoelectric bending actuator is presented. Then, the obtained nonlinear differential equations are solved by means of the method of multiple scales. In order to evaluate the suggested model, a set of experiments are conducted. Both frequency and phase responses are simultaneously considered to identify the dynamic nonlinear parameters. Moreover, in order to validate the accuracy of the proposed model, it is tested out of the identification range as well.

2. Nonlinear dynamic modeling

Fig. 1 depicts an actuator which is a symmetric bimorph cantilever with length l connected to a power supplier. The actuator is composed of an electrically inactive brass shim of density ρ_b with thickness t_b, and symmetric piezoceramic laminates of density ρ_p and thickness t_p. The cross section of the actuator is rectangular, and its width is Y.

2.1. Nonlinear constitutive equations

For a piezoelectric material, the conservative potential density can be expressed in terms of an electric enthalpy function. In order to describe the mechanical and electrical behaviors, and also, the electromechanical effects, this function consists of linear and nonlinear elastic, dielectric and coupling terms [20,21]. In order to model the nonlinear behavior, the conventional linear constitutive equations should be modified by nonlinear terms [25]. In this study, a nonlinear enthalpy function with the elastic nonlinearities up to fifth order is employed. Due to the low amplitude of the electric field near the natural frequency of the actuator, the nonlinear dielectric and coupling terms are presumed insignificant [21]. Also, because of the symmetry of the bimorph configuration, in the enthalpy function, the stiffness nonlinearities with odd power vanish. For a bending actuator that is actuated in the 31-mode, this function can be written in a reduced form as [26–29]

$$H_e = \frac{1}{2}c_{11}^E S_1^2 - e_{31}E_3 S_1 - \frac{1}{2}\varepsilon_{33}^S E_3^2 + \frac{1}{4}c_{111}S_1^4 + \frac{1}{6}c_{11111}S_1^6 \tag{1}$$

where c_{11}^{E} is the elastic modulus at a constant electric field, S_1 is the strain, c_{111} and c_{11111} are the nonlinear stiffness coefficients, e_{31} is the piezoelectric constant, E_3 is the electric field and ε_{33}^{S} is the permittivity at a constant strain. Regarding the electrical enthalpy density, the nonlinear constitutive relations are derived as

$$T_1 = \frac{\partial H_e}{\partial S_1} = c_{11}^{c} S_1 + e_{31} E_3 + c_{111} S_1^3 + c_{11111} S_1^5 \tag{2}$$

and

$$D_3 = -\frac{\partial H_e}{\partial E_3} = e_{31} E_3 + \varepsilon_{33}^{s} E_3 \tag{3}$$

2.2. Electrostatic energy expressions

The actuator understudy is modeled as an Euler–Bernoulli beam. Due to the small deflection of piezoelectric bending actuators, infinitesimal strain theory has been applied in which the following strain-displacement relation holds [20,21],

$$S_1 = -z\left(\frac{\partial^2 w}{\partial x^2}\right) \tag{4}$$

where $w = w(x,t)$ is the transverse deflection of the actuator. The actuator is made of three layers, and hence, the total kinetic energy is the summation of the kinetic energy of each layer. Moreover, due to actuator small deflection, it is assumed that the longitudinal and rotational motions are negligible [20,30]; therefore, the total kinetic energy of actuator can be cast in the following format,

$$T = \sum_{i=1}^{3} \int \frac{1}{2}\rho_i \left(\frac{\partial w}{\partial t}\right)^2 \mathrm{d}V_i \tag{5}$$

$$T = \frac{1}{2}\rho A_e \int_0^l \left(\frac{\partial w}{\partial t}\right)^2 \mathrm{d}x \tag{6}$$

where $\rho A_e = Y(\rho_b t_b + 2\rho_p t_p)$ is the mass per unit length of the actuator.

Moreover, the potential energy is stored in the actuator due to the bending strain energy of the brass substrate and the electrostatic enthalpy of the piezoceramic laminates. The potential strain energy within the brass substrate is linear and given by the following formulation,

$$U_b = \int\int\int \frac{1}{2} c_{11.b}^{E} S_1^2 \,\mathrm{d}V = \int\int\int -\frac{1}{2} c_{11.b}^{E} z^2 \left(\frac{\partial^2 w}{\partial x^2}\right)^2 \mathrm{d}V \tag{7}$$

where $c_{11.b}^{E}$ is the elastic modulus of brass substrate. Also, the potential energy of piezo laminates can be expressed as

$$\begin{aligned} U_e &= \int\int\int H_e \,\mathrm{d}V \\ &= \int\int\int \Bigg[-\frac{1}{2} c_{11.p}^{E} z^2 \left(\frac{\partial^2 w}{\partial x^2}\right)^2 + \frac{1}{4} c_{111} z^4 \left(\frac{\partial^2 w}{\partial x^2}\right)^4 + \frac{1}{6} c_{11111} z^6 \left(\frac{\partial^2 w}{\partial x^2}\right)^6 \\ &\quad - e_{31.i} E_{3.i} z \left(\frac{\partial^2 w}{\partial x^2}\right) + \frac{1}{2} \varepsilon_{33.i}^{S} E_{3.i}^2 \Bigg] \mathrm{d}V \end{aligned} \tag{8}$$

As a result, the total potential energy stored within the actuator is obtained as $U = U_b + U_e$, and upon integrating over the cross section, it yields:

$$\begin{aligned} U = \frac{1}{2} C I_e \int_0^l \left(\frac{\partial^2 w}{\partial x^2}\right)^2 \mathrm{d}x - \int \left[\alpha \left(\frac{\partial^2 w}{\partial x^2}\right)^4 + \beta \left(\frac{\partial^2 w}{\partial x^2}\right)^6\right] \mathrm{d}x - \frac{1}{2} \sum_{i=1}^{3} e_{31.i} Y_i \left[t_{i.o}^2 - t_{i.u}^2\right] \int_0^l E_3 \left(\frac{\partial^2 w}{\partial x^2}\right) \mathrm{d}x \\ + \sum_{i=1}^{3} \frac{1}{2} \varepsilon_{33.i}^{S} [t_{i.o} - t_{i.u}] w_i \int_0^l E_{3.i}^2 \,\mathrm{d}x \end{aligned} \tag{9}$$

in which o and u denote the upper and lower side of each layer and the coefficients are defined as,

$$CI_e = c_b I_b + c_p I_p = \frac{c_b Y t^3}{12} + \frac{1}{6} Y c_{11}^E \left[4t_p^3 + 6t_p^2 t_b + 3t_b^2 t_p\right] \tag{10}$$

$$\alpha = \frac{Y}{160} c_{111} \left(5t_b^4 t_p + 20t_b^3 t_p^2 + 40t_b^2 t_p^3 + 40t_b t_p^4 + 16t_p^5\right) \tag{11}$$

$$\beta = \frac{Y}{1344} c_{11111} \left(7t_b^6 t_p + 42t_b^5 t_p^2 + 140t_b^4 t_p^3 + 280t_b^3 t_p^4 + 336t_b^2 t_p^5 + 224t_b t_p^6 + 64t_p^5\right) \tag{12}$$

The first term in Eq. (9) represents the linear bending energy of substrate, and the terms which are proportional to α and β represent the nonlinear stress-strain behavior of the piezoceramic laminates.

2.3. Continuous nonlinear dynamic model

In order to drive the governing equations of the actuator, the Hamilton's principle is employed. According to the Hamilton's principle the variation of the Lagrangian minus the non-conservative work attains a stationary value between two time instances, namely,

$$\int_{t_0}^{t_1} (\delta L - \delta W)\, \mathrm{d}t = 0 \tag{13}$$

where δ denotes the variational derivative, and the Lagrangian function is defined as $L = T - U$,

$$L = f\left(\frac{\partial w}{\partial t}, \frac{\partial^2 w}{\partial x^2}, E_{3.i}\right) \tag{14}$$

Here, the non-conservative work term consists of the work done by the applied voltage and the dissipative frictional forces, namely,

$$W = -\int_0^l \mu \left(\frac{\partial w}{\partial t}\right) w\, \mathrm{d}x - \sum_{i=1}^{3} \int_{t_{i.u}}^{t_{i.o}} \int_0^Y \int_0^l \sigma \left(\frac{\partial U}{\partial z}\right) \mathrm{d}x\, \mathrm{d}y\, \mathrm{d}z \tag{15}$$

where μ is the coefficient of friction and σ is the surface charge density.

Also, a linear relation is assumed between the electric field and voltage as follows [20,21]:

$$E_3 = \frac{V_3(x,t)}{t_p} \tag{16}$$

in which

$$V_3(x,t) = V(t)\left[H(x) - H(x-l)\right] \tag{17}$$

where $H(x)$ is the Heaviside function.

Substituting Eqs. (15)–(17) into Eq. (13), applying the calculus of variations, and using the integration by parts, the nonlinear equation of motion of the actuator is obtained as follows:

$$CI_e w'''' + \rho A_e \ddot{w} + \mu \dot{w} + 12\alpha \left(2w'' w'''^2 + w'''' w''^2\right) + 30\beta (6w''^3 w'''^2 + w'''' w''^4) = -M_p V(t) \frac{\mathrm{d}}{\mathrm{d}x}\delta(x-l) \tag{18}$$

in which

$$M_p = Y e_{31} \left(t_p + t_b\right) \tag{19}$$

and $\delta(x)$ refers to the Dirac delta function, which has appeared due to the differentiation of the Heaviside function $H(x)$ with respect to x.

2.4. Distributed parameters model

In order to discretize the obtained continuous dynamic model, Galerkin's method is utilized. For this purpose, the transverse deflection is approximated as a summation of eigenfunctions, which includes the multiplication of generalized displacements with the corresponding orthogonal basis functions, namely,

$$w\,(x.t) = \sum_{i=0}^{n} \varphi_i\,(x)\,q_i(t) \tag{20}$$

In this study, the actuator is excited harmonically with a frequency near the fundamental natural frequency, and hence, the single mode assumption can be made. This simplification is proven to be sufficiently accurate in the case of steady-state oscillations [20,23]. Also, it should be noted that the foregoing assumption can be valid when there is not any internal resonance in the system. Nevertheless, the single mode assumption is not valid, and the internal resonance effect should be taken into account in the dynamic behavior analysis [29]. The corresponding single basis function is the first vibrational mode shape function of an Euler–Bernoulli undamped beam with fixed-free boundary conditions, namely,

$$\begin{aligned} &\varphi_1\,(x) = \eta_1 \overline{\varphi}_1\,(x) \\ &\overline{\varphi}_1\,(x) = [\cos\,(\gamma_1 x) - \cosh(\gamma_1 x)] - \frac{\cos\,(\gamma_1 l) + \cosh\,(\gamma_1 l)}{\sin\,(\gamma_1 l) + \sinh\,(\gamma_1 l)}[\sin\,(\gamma_1 x) - \sinh\,(\gamma_1 x)] \end{aligned} \tag{21}$$

where

$$\gamma_1 = 1.8751 \tag{22}$$

$$\omega_1 = \gamma_1^2 \sqrt{\frac{C I_e}{\rho A_e}} \tag{23}$$

$$\eta_1 = \frac{1}{\sqrt{\int_0^l \rho A_e \overline{\varphi}_1^2\,(x)\,\mathrm{d}x}} \tag{24}$$

Moreover, the orthogonality conditions between the base functions can be written as follows:

$$\int_0^l \rho A_e \varphi_m\,(x)\,\varphi_n\,(x)\,\mathrm{d}x = \delta_{mn} \tag{25}$$

$$\int_0^l \varphi_m\,(x)\,\frac{\partial^2}{\partial x^2}\left((C I_e)\,\frac{\partial^2 \varphi_n\,(x)}{\partial x^2}\right)\mathrm{d}x = \omega_m^2 \delta_{mn} \tag{26}$$

where ω_m is the mth undamped natural frequency and δ_{mn} is the Kronecker delta function. By substituting Eq. (20) into Eq. (18), multiplying by $\varphi_n\,(x)$ and integrating over the actuator length, the nonlinear ordinary differential equation of motion near the fundamental frequency is obtained as

$$\ddot{q}_i + 2\xi_i \omega_i \dot{q}_i + \omega_i^2 q_i + k_1 q^3 + k_2 q^5 = -M_p V\,(t) \int_0^l \varphi_j(x)\,\frac{\mathrm{d}\delta}{\mathrm{d}x}(x-l) \tag{27}$$

whose coefficients are defined in the sequel,

$$k_1 = 12\alpha \int_0^l \varphi \left[\varphi''^2 \varphi'''' + 2\varphi'' \varphi'''^2\right]\mathrm{d}x \tag{28}$$

$$k_2 = 30\beta \int_0^l \varphi \left[6\varphi''^3 \varphi'''^2 + \varphi''^4 \varphi''''\right]\mathrm{d}x \tag{29}$$

Based on the following identity equation,

$$\int_a^c \delta^{(n)}\,(x-b)\,f\,(x)\,\mathrm{d}x = (-1)^n\,f^{(n)}\,(b) \quad a \le b \le c \tag{30}$$

Equation (27) can be reformulated into the following format,

$$\ddot{q} + 2\xi\omega_n \dot{q} + \omega_n^2 q + k_1 q^3 + k_2 q^5 = m_{pi} V\,(t) \tag{31}$$

where

$$m_{\mathrm{pi}} = -M_{\mathrm{p}} \frac{\partial \varphi_i(x)}{\partial x}\bigg|_{x=l} \tag{32}$$

According to the literature, a piezoelectric bending actuator that is driven by a weak electric field exhibits nonlinear damping behavior [20,21,30]; therefore, a nonlinear damping model should be considered. In this study, a nonlinear damping model that was first introduced by Stanton et al. in [21] is incorporated. This model is defined as

$$D = \mu + \mu_1 q^2 \tag{33}$$

As a result, the nonlinear differential equation of motion for the actuator under study becomes

$$\ddot{q} + (\mu + \mu_1 q^2)\dot{q} + \omega_n^2 q + k_1 q^3 + k_2 q^5 = m_{\mathrm{pi}} V(t) \tag{34}$$

where

$$\mu = 2\xi\omega_n \tag{35}$$

3. Dynamic response analysis

In this section, the nonlinear equation of motion of the actuator, i.e. Eq. (34), is solved analytically by means of a perturbation based method called multiple scales [31]. In this method, in order to describe a weak nonlinear behavior, displacement is expanded into the summation of the terms that are proportional to a small expansion parameter denoted by ε and the corresponding independent time scales,

$$q(t) = \sum_{k=0}^{1} \varepsilon^k x_k(T_0.T_1) = x_0 + \varepsilon x_1 \tag{36}$$

The parameter ε is, in fact, a bookkeeping parameter that will be set to unity at the end of the analysis. Therefore, instead of determining q as a function of t, the variable q is determined as a function of different time scales, namely, T_0, T_1, $T_2 \ldots$ These time scales are defined as

$$T_0 = t \quad T_1 = \varepsilon t \quad T_2 = \varepsilon^2 t \quad T_3 = \varepsilon^3 t \quad \ldots \tag{37}$$

This guarantees that the dependence of q on t and ε occurs at different scales. To this end, the independent variable in Eq. (34) can be changed via the chain rule, namely,

$$\begin{aligned} \frac{\mathrm{d}}{\mathrm{d}t} &= \frac{\partial}{\partial T_0} + \varepsilon \frac{\partial}{\partial T_1} + \cdots = D_0 + \varepsilon D_1 + \ldots \\ \frac{\mathrm{d}^2}{\mathrm{d}t^2} &= \frac{\partial^2}{\partial T_0^2} + 2\varepsilon \frac{\partial^2}{\partial T_0 \partial T_1} + \cdots = D_0^2 + 2\varepsilon D_0 D_1 + \ldots \end{aligned} \tag{38}$$

Also, all nonlinear terms and the harmonic force are balanced to include the first-order correction, namely,

$$\begin{aligned} \mu_i &= \varepsilon \overline{\mu}_i \\ k_i &= \varepsilon \overline{k}_i \\ V(t) &= \varepsilon V_a(t) \end{aligned} \tag{39}$$

By substitution of Eq. (39) into Eq. (34) and equating the coefficient of ε^0 and ε, one obtains the following equations,

$$D_0^2 q_0 + \omega_n^2 q_0 = 0 \tag{40}$$

$$D_0^2 q_1 + \omega_n^2 q_1 = -2D_0 D_1 q_1 - \left(\overline{\mu} + \overline{\mu}_1 q_0^2\right) D_0 q_0 - \overline{k}_1 q_0^3 - \overline{k} q_0^5 + V_a(t) \tag{41}$$

The harmonic excitation can be written as

$$V_a = \frac{1}{2} V \mathrm{e}^{\mathrm{i}\omega T_0} \tag{42}$$

where ω is the excitation frequency. To study the behavior of a system around the first natural frequency, the excitation frequency can be expressed in terms of natural frequency of the system, such as

$$\omega = \omega_n(1 + \sigma\varepsilon) \tag{43}$$

where σ is a detuning parameter. The general solution to Eq. (40) can be expressed as

$$q_0 = A(T_1)\mathrm{e}^{\mathrm{i}\omega_n T_0} + \overline{A}(T_1)\mathrm{e}^{-\mathrm{i}\omega_n T_0} = A(T_1)\mathrm{e}^{\mathrm{i}\omega_n T_0} + cc \tag{44}$$

where cc indicates the complex conjugate term. As the derivation in Eq. (40) is with respect to T_0, the amplitude A is not a constant parameter, but a function of slow-scale T_1. By substituting q_0 into Eq. (41), disregarding higher harmonics and eliminating the secular terms yields

$$2\mathrm{i}\omega_n A' + \overline{\mu}\mathrm{i}\omega_n A + \overline{\mu}_1\mathrm{i}\omega_n A^2\overline{A} + 3\overline{k}_1 A^2\overline{A} + 10\overline{k}_2 A^3\overline{A}^2 - \frac{1}{2}V\mathrm{e}^{\mathrm{i}\omega_n\sigma T_1} = 0 \tag{45}$$

The amplitude $A(T_1)$ can be defined in terms of the polar coordinates,

$$A(T_1) = \frac{1}{2}\alpha(T_1)\mathrm{e}^{\mathrm{i}\beta(T_1)} \tag{46}$$

And thus, by substitution of Eq. (46) into Eq. (45), the following equations yield:

$$\omega_n\dot{\alpha} = -\frac{1}{2}\alpha\omega_n\overline{\mu} - \frac{1}{8}\omega_n\alpha^3\overline{\mu}_1 + \frac{1}{2}V\sin(\sigma T_1 - \beta) \tag{47}$$

$$-\alpha\omega_n\dot{\beta} = -\frac{3}{8}\overline{k}_1\alpha^3 - \frac{10}{32}\overline{k}_2\alpha^5 + \frac{1}{2}V\cos(\sigma T_1 - \beta) \tag{48}$$

In order to eliminate the explicit dependence on T_1, a new variable is introduced below

$$\gamma = \sigma\omega_n T_1 - \beta \tag{49}$$

By substituting Eq. (49) into Eqs. (47) and (48), the following equations are obtained,

$$\dot{\alpha}\omega_n = -\frac{1}{2}\alpha\omega_n\overline{\mu} - \frac{1}{8}\omega_n\alpha^3\overline{\mu}_1 + \frac{1}{2}V\sin(\gamma) \tag{50}$$

$$\alpha\omega_n\dot{\gamma} = +\sigma\omega_n^2\alpha - \frac{3}{8}\overline{k}_1\alpha^3 - \frac{10}{32}\overline{k}_2\alpha^5 + \frac{1}{2}V\cos(\gamma) \tag{51}$$

In this study, the steady-state frequency response of the actuator is required. As the variables α and γ attain a constant magnitude in the steady-state vibration of the actuator, their derivatives $\dot{\alpha}$ and $\dot{\gamma}$ vanish. Thus, Eqs. (50) and (51) can be reformed to the following formats,

$$\frac{1}{2}\alpha\omega_n\overline{\mu} + \frac{1}{8}\omega_n\alpha^3\overline{\mu}_1 = \frac{1}{2}V\sin(\gamma) \tag{52}$$

$$-\sigma\omega_n^2\alpha + \frac{3}{8}\overline{k}_1\alpha^3 + \frac{10}{32}\overline{k}_2\alpha^5 = \frac{1}{2}V\cos(\gamma) \tag{53}$$

The phase can be eliminated by squaring and adding both sides of the equations above, namely,

$$\left(\frac{1}{2}\overline{\mu}\omega_n\alpha + \frac{1}{8}\overline{\mu}_1\omega_n\alpha^3\right)^2 + \left(\sigma\omega_n^2\alpha - \frac{3}{8}\overline{k}_1\alpha^2 - \frac{10}{32}\overline{k}_2\alpha^4\right)^2\alpha^2 = \frac{1}{4}V^2 \tag{54}$$

Eq. (54) can be used to calculate the amplitude of the steady-state vibration. In addition, the phase response can be achieved by calculating the steady-state response of Eq. (48).

4. Experimental analysis

4.1. Experimental setup

In this section, the validity of the suggested mathematical framework is experimentally evaluated by means of a bimorph piezoelectric actuator (T226-H4-203X), which consists of a brass substrate that is symmetrically laminated with two lead zirconate titanite layers (series connection). The actuator's properties are listed in Table 1.

Fig. 2 shows the experimental set-up in which an amplifier (EPA-104-230) from Piezo System Company (Woburn, MA, USA) provides the required voltages. Two data acquisition cards (PCI-1710) and (PCI-1716) capture data with a frequency of 20 kHz. Also, a laser displacement sensor (Micro-Epsilon optoNCDT 2300) measures the deflection with a resolution of 10 nm.

Table 1
Geometric and material properties of the PZT-5H bimorph bending actuator.

Parameters	PZT-5H	Brass
Length (l) (mm)	24.53	24.53
Width (Y) (mm)	6.4	6.4
Thickness (t) (mm)	0.265	0.140
Mass density (ρ) (kg/m^3)	7500	9000
Elastic modulus (c_E, c_b) (GPa)	51.51	105
Piezoelectric constant (e_{31}) (C/m^2)	−13.11	–
Permittivity constant (ε_{33}) (nF/m)	25.5	–

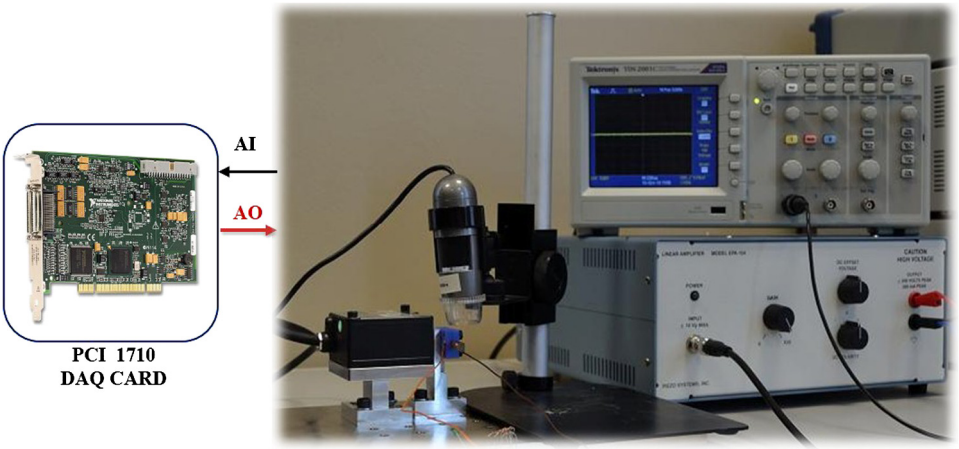

Fig. 2. The experimental setup.

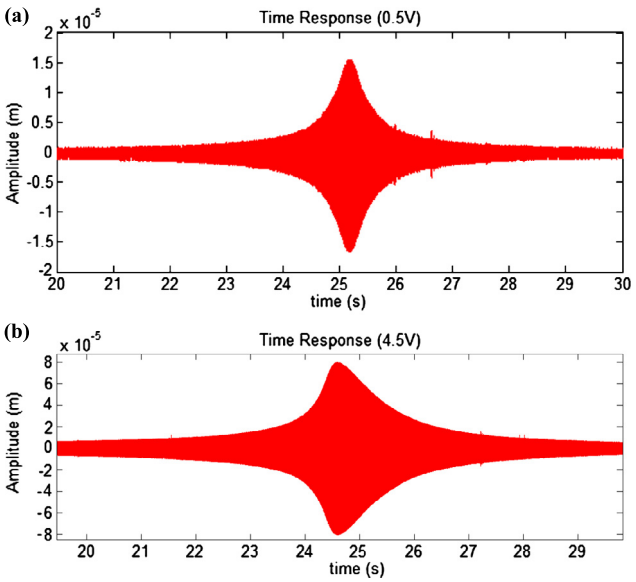

Fig. 3. Actuator time responses for two levels of chirp input voltages. (a) 0.5 V; (b) 4.5 V.

4.2. Linear dynamic identification

First of all, in order to identify the linear damping ratio, a series of experiments were conducted. The identification is performed using a chirp signal with a constant amplitude, a duration of 60 s, and a frequency range from 0.1 to 1000 Hz. The sampling time is set to 0.0001 s. Fig. 3 shows the time response of the actuator, which is sensed at a point close to the tip ($x_t \approx 23.46$ mm) at two input voltages.

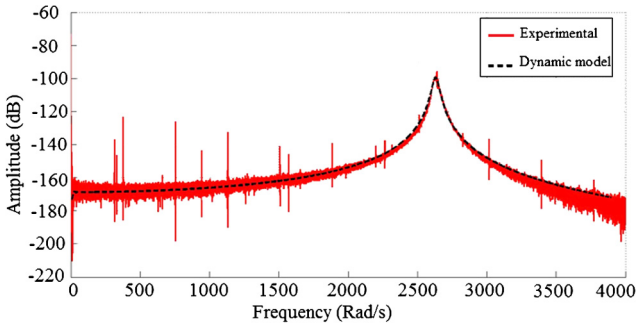

Fig. 4. Frequency response for V = 0.5 V obtained by experiment and analytical model.

It is clear that the actuator depicts the nonlinear behavior by increasing the input voltage. Therefore, to decrease the effects of nonlinear behaviors on the vibration of the actuator and minimizing the error of linear modeling, a low-amplitude input voltage of 0.5 V is applied. Finally, a fast Fourier transform (FFT) algorithm is utilized to compare the experimental data with the ones obtained with the linear theory. As a result, the first natural frequency of actuator is obtained as 2637 rad/s with the linear damping ratio of $\xi = 0.0085$. Fig. 4 illustrates the correspondence between the linear model for $\xi = 0.0085$ and the experimental data for a low-amplitude excitation.

In order to accurately describe the dynamic behavior of the piezoelectric actuator, one needs to identify the nonlinear parameters of Eq. (34) as well. For this purpose, a solution to the nonlinear equation of motion of the actuator should be first obtained, which is explained in the sequel.

4.3. Nonlinear dynamic identification

In order to validate the proposed dynamic model for the bimorph piezoelectric actuator, and also to identify the nonlinear parameters, an experiment is conducted, in which the actuator is excited by means of a sinusoidal input signal. As the obtained fundamental natural frequency of the actuator is 2637 rad/s, the experimental data are acquired at frequencies near the resonance, such as 2512, 2580, 2637, 2680, and 2736 rad/s. The laser displacement sensor is set almost on the tip of the actuator ($x_t \approx 23.46$ mm), and the steady-state displacements are recorded for nine different input voltages with a sampling time of 0.0001 s. It is noteworthy to mention that each amplitude on the frequency response plot is the average of all peak displacements over the time response of the actuator. Starting with initial values for unknown nonlinear parameters, the steady-state phase and the amplitude of the actuator displacement are obtained by resorting to Eqs. (54) and (48). In order to ensure that the suggested model accurately describes the phase of the system, the phase values are also obtained experimentally at different frequencies and amplitudes. However, the time delay, which is caused by the data acquisition card, significantly affect the data, and thus, it should be eliminated. In this regard, the value of phase difference which is caused by the equipment is first experimentally measured, and then, it is subtracted from the total phase difference at each corresponding frequency. It is noteworthy to mention that the main target of this study is to evaluate the nonlinear parameters by considering the amplitude and the phase frequency responses simultaneously. The identification process results in the following values for the unknown nonlinear parameters,

$$k_1 = -6.94 \times 10^{17}$$
$$k_2 = 1.443 \times 10^{28}$$
$$\mu_1 = 6.28 \times 10^{13}$$

Fig. 5 shows the actuator vibration amplitude at frequencies around the first resonance. Small triangles refer to the experiments, and the solid lines are obtained from the solution to Eq. (54) for different input voltages. The results ensure that the nonlinear parameters are identified correctly, and also that the suggested model properly predicts the vibration amplitude for different input voltages.

To evaluate the accuracy of the dynamic modeling and its identification, the theoretical and experimental phase responses have been illustrated in Fig. 6 for three different input voltages. As it is observed, the phase responses that are obtained from experiments are in good agreement with the theoretical results.

In order to better clarify the difference between a linear and a nonlinear model, the corresponding phase responses are also shown in Fig. 7.

It is obvious that, like for the amplitude-frequency response, the actuator nonlinearity can make a distortion in the phase-frequency response as well. Moreover, as it is apparent from the results, the responses that are obtained by the linear model are significantly different from that of nonlinear model, and hence, the necessity of an accurate nonlinear modeling

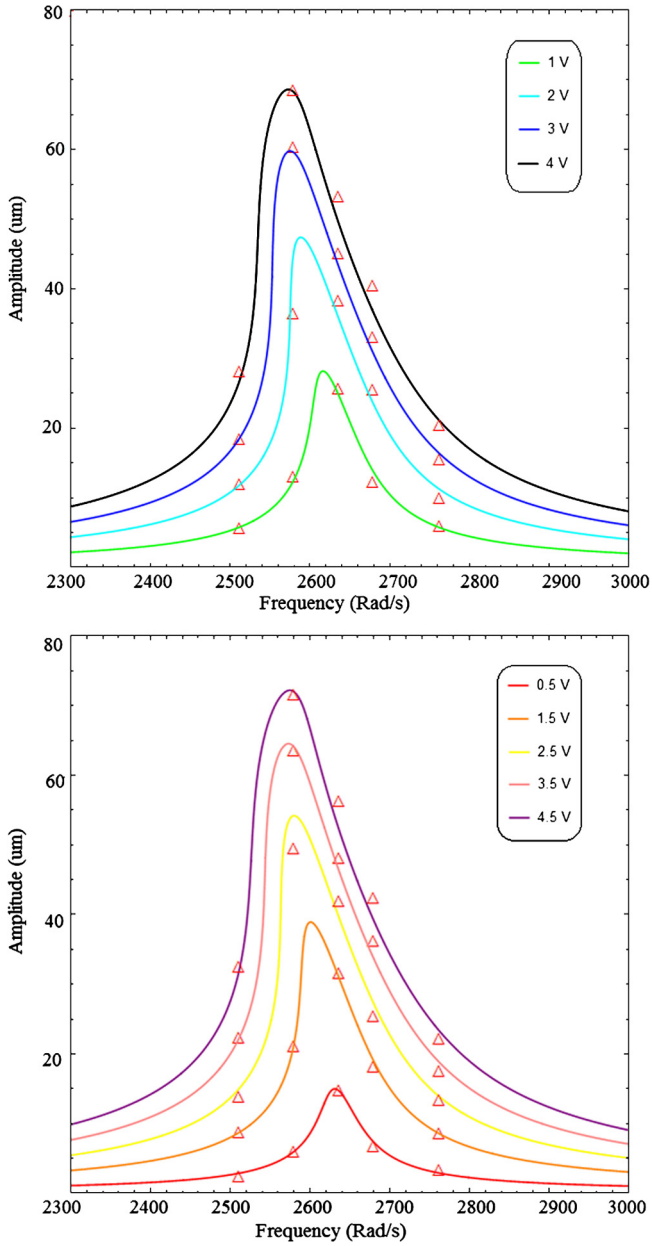

Fig. 5. Identification results for the actuator vibration amplitude at different input voltages. Triangles: experiments; solid lines: nonlinear model.

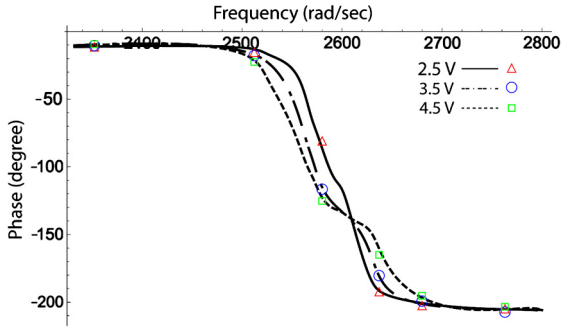

Fig. 6. Identification results for the actuator vibration phase at different input voltages. Triangles: experiments; Lines: nonlinear model.

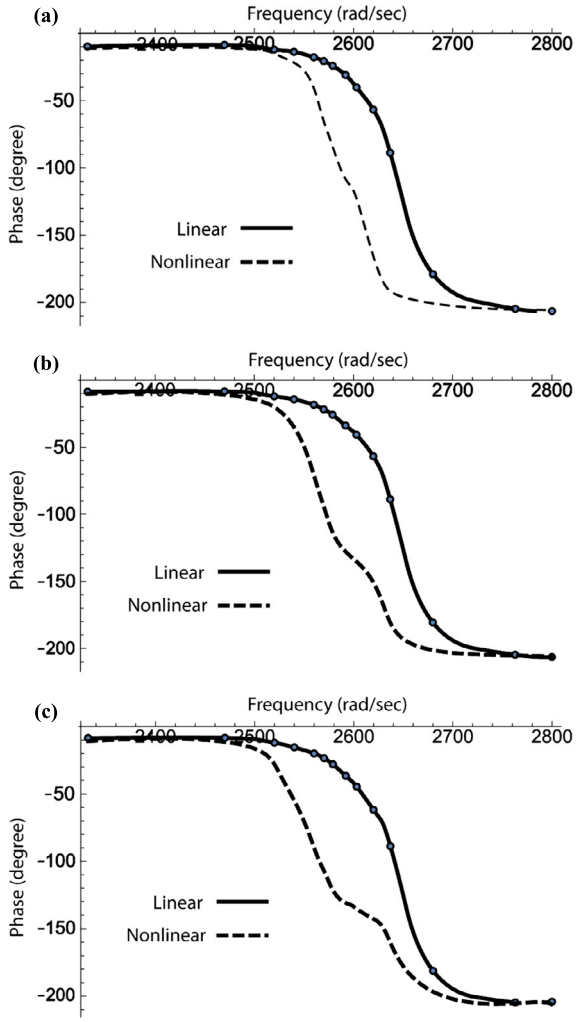

Fig. 7. Comparison of phase responses for linear and nonlinear models for different input voltages. (a) 2.5 V; (b) 3.5 V; (c) 4.5 V.

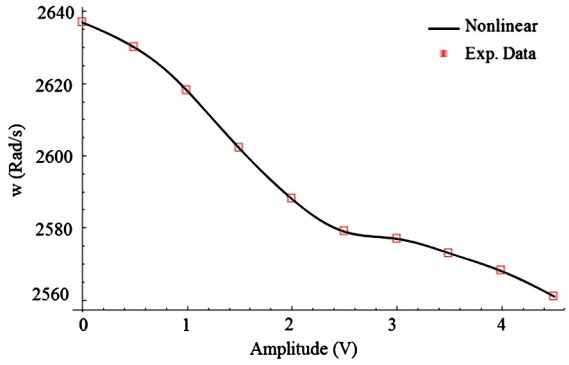

Fig. 8. Frequency drift of the peak amplitude for various excitation voltages.

is justified. In this study, with an elastic nonlinearity up to the fifth order and only one nonlinear damping parameter, the nonlinear behavior of the piezoelectric actuator is accurately predicted.

The piezoelectric actuators are generally designed to work at the resonant condition; therefore, as it was depicted, a linear model fails to precisely describe the dynamic behavior. Fig. 8 shows the frequency drift of the peak amplitude for different input voltages.

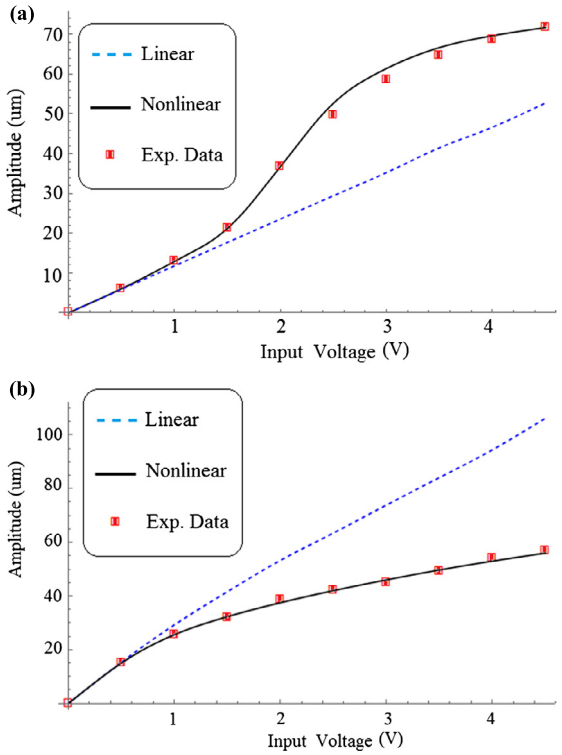

Fig. 9. The input voltage effect on the vibration amplitude in two frequencies below and above the first resonance (a) $\omega = 2580$ rad/s, (b) $\omega = 2637$ rad/s.

It should be noted that, in case of linear systems, there is no frequency drift, and the corresponding plot is a horizontal line. In other words, the natural frequency of a linear system does not depend on the amplitude of excitation. However, in nonlinear systems, by increasing the amplitude of excitation the natural frequency can be increased or decreased, which is called hardening or softening behavior, respectively. As it is shown in Fig. 8, in the present case study, the actuator presents softening behavior. The deviation of the linear model from the nonlinear one, at special frequencies below and above resonance, is illustrated in Fig. 9. In a nonlinear system with softening behavior, at frequencies below the fundamental natural frequency, by increasing the amplitude of excitation, the response amplitude is increased with a higher rate than the one in the corresponding linear model (Fig. 9a). However, at frequencies above the fundamental natural frequency, this rate becomes lower than the linear model counterpart (Fig. 9b).

In the aforementioned modeling, the nonlinear parameters are identified by considering the phase and amplitude of displacement simultaneously. Therefore, as a matter of fact, it is expected that the suggested model predicts the behavior of the actuator with any physically possible higher amplitude. To verify the foregoing claim, the frequency responses of actuator at higher input voltages, such as 6, 8, and 10 V, are also investigated and compared with the corresponding experimental data. Fig. 10 depicts the theoretical amplitude responses achieved by the previously identified nonlinear parameters in comparison with the ones obtained experimentally. In order to check the fidelity of the model, in the experiment, the input voltage is increased up to two times of what was considered in the identification study; as it is apparent, the proposed model can still predict the behavior of the system accurately.

5. Conclusions

In this work, a nonlinear mathematical framework was developed and experimentally validated for a piezoelectric bimorph actuator. The actuator was excited from low to high electrical voltages in its first bending mode. The nonlinear mathematical framework was obtained using Hamilton's principles, Galerkin's method, and the single mode assumption. The obtained nonlinear equation was solved by resorting to the multiple scales method. The nonlinear parameters were identified by applying voltages between 0.5 to 4.5 V, and the results were compared with the experimental data. The linear parameter identification was done using MATLAB FFT algorithms and the nonlinear parameter identification was conducted by considering amplitude and phase frequency responses of the actuator simultaneously. In the identification domain, the suggested model accurately predicts the overall dynamic behavior of the actuator for near-resonant actuation with the maximum error of 7% and an average error of 5.5% [16].

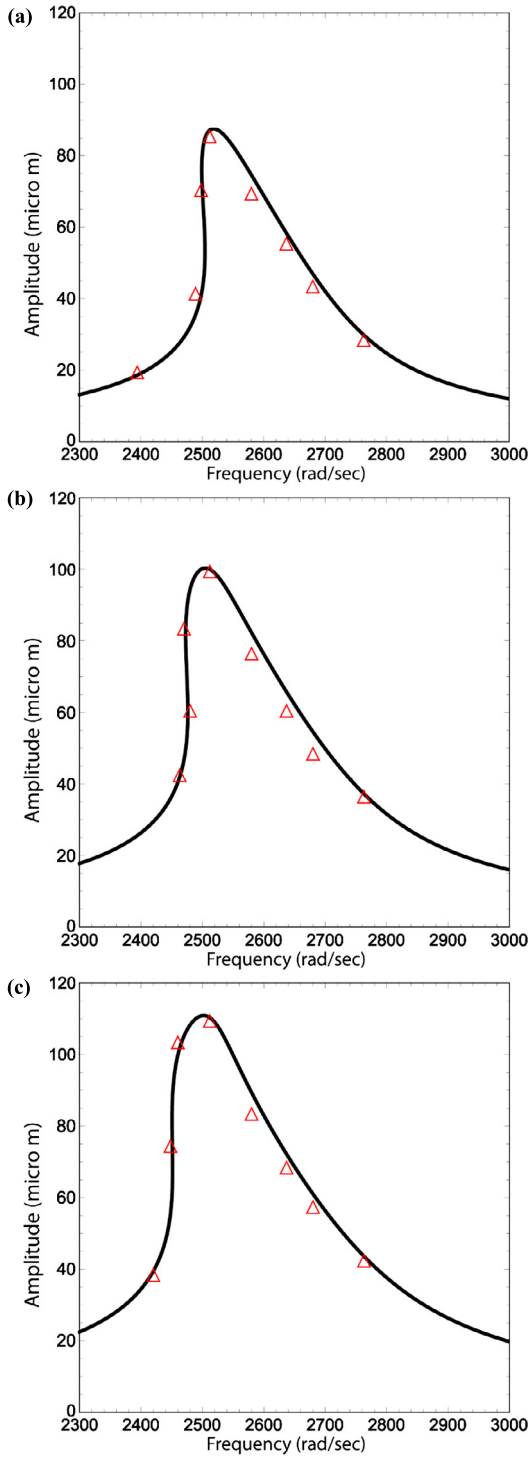

Fig. 10. Evaluation of the identified nonlinear model in higher input voltages; triangles: experiments; solid lines: nonlinear model: (a) 6 V; (b) 8 V; (c) 10 V.

References

[1] N. Hosseini, A.P. Nievergelt, J.D. Adams, V.T. Stavrov, G.E. Fantner, A monolithic MEMS position sensor for closed-loop high-speed atomic force microscopy, Nanotechnology 27 (2016) 135705.

[2] J. Lee, W. Choi, Y.K. Yoo, K.S. Hwang, S.M. Lee, S. Kang, et al., A micro-fabricated force sensor using an all thin film piezoelectric active sensor, Sensors (Basel) 14 (2014) 22199–22207.

[3] G. Yan, H. Ying, Y. Linguo, H. Jisheng, H. Youjin, Y. Yanchun, et al., Piezoelectric sensor for micro mass detection, in: 2016 13th International Computer Conference on Wavelet Active Media Technology and Information Processing (ICCWAMTIP), 2016, pp. 111–113.
[4] H. Abdelmoula, S. Zimmerman, A. Abdelkefi, Accurate modeling, comparative analysis, and performance enhancement of broadband piezoelectric energy harvesters with single and dual magnetic forces, Int. J. Non-Linear Mech. 95 (2017) 355–363.
[5] C. Dagdeviren, P. Joe, O.L. Tuzman, K.-I. Park, K.J. Lee, Y. Shi, et al., Recent progress in flexible and stretchable piezoelectric devices for mechanical energy harvesting, sensing and actuation, Extrem. Mech. Lett. 9 (2016) 269–281.
[6] H. Ghafarirad, S.M. Rezaei, M. Zareinejad, A.A.D. Sarhan, Disturbance rejection-based robust control for micropositioning of piezoelectric actuators, C. R. Mecanique 342 (2014) 32–45.
[7] R.K. Jain, S. Majumder, B. Ghosh, S. Saha, Design and manufacturing of mobile micro manipulation system with a compliant piezoelectric actuator based micro gripper, J. Manuf. Syst. 35 (2015) 76–91.
[8] H.-K. Ma, W.-F. Luo, J.-Y. Lin, Development of a piezoelectric micropump with novel separable design for medical applications, Sens. Actuators A, Phys. 236 (2015) 57–66.
[9] X. Chen, Z. Chen, X. Li, L. Shan, W. Sun, X. Wang, et al., A spiral motion piezoelectric micromotor for autofocus and auto zoom in a medical endoscope, Appl. Phys. Lett. 108 (2016) 052902.
[10] M. Rakotondrabe, I.A. Ivan, S. Khadraoui, P. Lutz, N. Chaillet, Simultaneous displacement/force self-sensing in piezoelectric actuators and applications to robust control, IEEE/ASME Trans. Mechatron. 20 (2015) 519–531.
[11] A. Mystkowski, A.P. Koszewnik, Mu-Synthesis robust control of 3D bar structure vibration using piezo-stack actuators, Mech. Syst. Signal Process. 78 (2016) 18–27.
[12] D. Mazeika, P. Vasiljev, S. Borodinas, R. Bareikis, Y. Yang, Small size piezoelectric impact drive actuator with rectangular bimorphs, Sens. Actuators A, Phys. 280 (2018) 76–84.
[13] A. Erturk, D.J. Inman, An experimentally validated bimorph cantilever model for piezoelectric energy harvesting from base excitations, Smart Mater. Struct. 18 (2009) 025009.
[14] A. Erturk, D.J. Inman, A distributed parameter electromechanical model for cantilevered piezoelectric energy harvesters, J. Vib. Acoust. 130 (2008) 041002.
[15] H. Ghafarirad, S.M. Rezaei, A.A.D. Sarhan, M. Zareinejad, Continuous dynamic modelling of bimorph piezoelectric cantilevered actuators considering hysteresis effect and dynamic behaviour analysis, Math. Comput. Model. Dyn. Syst. 21 (2) (2015) 130–152, https://doi.org/10.1080/13873954.2014.906472.
[16] R. Hosseini, M. Hamedi, A. Ebrahimi Mamaghani, H.C. Kim, J. Kim, J. Dayou, Parameter identification of partially covered piezoelectric cantilever power scavenger based on the coupled distributed parameter solution, Int. J. Smart Nano Mater. 8 (2017) 110–124.
[17] S.S. Raju, M. Umapathy, G. Uma, High-output piezoelectric energy harvester using tapered beam with cavity, J. Intell. Mater. Syst. Struct. 29 (2018) 800–815.
[18] H. Ghafarirad, S.M. Rezaei, M. Zareinejad, M. Hamdi, R.J. Ansari, Robust control with unknown dynamic estimation for multi-axial piezoelectric actuators with coupled dynamics, C. R. Mecanique 340 (2012) 646–660.
[19] P.P. Chao, P.-Y. Liao, M.-Y. Tsai, C.-T. Lin, Robust control design for precision positioning of a generic piezoelectric system with consideration of microscopic hysteresis effects, Microsyst. Technol. 17 (2011) 1009–1023.
[20] S.C. Stanton, A. Erturk, B.P. Mann, D.J. Inman, Nonlinear piezoelectricity in electroelastic energy harvesters: modeling and experimental identification, J. Appl. Phys. 108 (2010) 074903.
[21] S.C. Stanton, A. Erturk, B.P. Mann, E.H. Dowell, D.J. Inman, Nonlinear nonconservative behavior and modeling of piezoelectric energy harvesters including proof mass effects, J. Intell. Mater. Syst. Struct. 23 (2012) 183–199.
[22] S. Leadenham, A. Erturk, Nonlinear M-shaped broadband piezoelectric energy harvester for very low base accelerations: primary and secondary resonances, Smart Mater. Struct. 24 (2015) 055021.
[23] D. Tan, P. Yavarow, A. Erturk, Nonlinear elastodynamics of piezoelectric macro-fiber composites with interdigitated electrodes for resonant actuation, Compos. Struct. 187 (2018) 137–143.
[24] R.G. Ballas, Piezoelectric Multilayer Beam Bending Actuators Static and Dynamic Behavior and Aspects of Sensor Integration, Springer, New York, 2007.
[25] A. Chattopadhyay, C.E. Seeley, A higher order theory for modeling composite laminates with induced strain actuators, Composites, Part B, Eng. 28 (1997) 243–252.
[26] A. Abdelkefi, A.H. Nayfeh, M.R. Hajj, Effects of nonlinear piezoelectric coupling on energy harvesters under direct excitation, Nonlinear Dyn. 67 (2012) 1221–1232.
[27] A. Abdelkefi, A.H. Nayfeh, M.R. Hajj, Global nonlinear distributed-parameter model of parametrically excited piezoelectric energy harvesters, Nonlinear Dyn. 67 (2012) 1147–1160.
[28] K. Mam, M. Peigney, D. Siegert, Finite strain effects in piezoelectric energy harvesters under direct and parametric excitations, J. Sound Vib. 389 (2017) 411–437.
[29] V. Guillot, A.T. Savadkoohi, C.-H. Lamarque, Analysis of a reduced-order nonlinear model of a multi-physics beam, Nonlinear Dyn. 97 (2) (2019) 1371–1401.
[30] S.C. Stanton, A. Erturk, B.P. Mann, D.J. Inman, Resonant manifestation of intrinsic nonlinearity within electroelastic micropower generators, Appl. Phys. Lett. 97 (2010) 254101.
[31] A.H. Nayfeh, D.T. Mook, Nonlinear Oscillations, John Wiley & Sons, 2008.